

In situ switching of photoinduced electron transfer direction by regulating redox state in fullerene-based dyads

Yongqiang Chai, Xiaolong Liu, Bo Wu, Liping Liu, Zhuan Wang, Yuxiang Weng, and Chunru Wang

J. Am. Chem. Soc., **Just Accepted Manuscript** • DOI: 10.1021/jacs.9b13376 • Publication Date (Web): 07 Feb 2020

Downloaded from pubs.acs.org on February 7, 2020

Just Accepted

“Just Accepted” manuscripts have been peer-reviewed and accepted for publication. They are posted online prior to technical editing, formatting for publication and author proofing. The American Chemical Society provides “Just Accepted” as a service to the research community to expedite the dissemination of scientific material as soon as possible after acceptance. “Just Accepted” manuscripts appear in full in PDF format accompanied by an HTML abstract. “Just Accepted” manuscripts have been fully peer reviewed, but should not be considered the official version of record. They are citable by the Digital Object Identifier (DOI®). “Just Accepted” is an optional service offered to authors. Therefore, the “Just Accepted” Web site may not include all articles that will be published in the journal. After a manuscript is technically edited and formatted, it will be removed from the “Just Accepted” Web site and published as an ASAP article. Note that technical editing may introduce minor changes to the manuscript text and/or graphics which could affect content, and all legal disclaimers and ethical guidelines that apply to the journal pertain. ACS cannot be held responsible for errors or consequences arising from the use of information contained in these “Just Accepted” manuscripts.

In situ switching of photoinduced electron transfer direction by regulating redox state in fullerene-based dyads

Yongqiang Chai, †§^{||} Xiaolong Liu, †^{||} Bo Wu, *† Liping Liu, †§ Zhuan Wang, ‡ Yuxiang Weng *‡§ and Chunru Wang *†

[†]Beijing National Laboratory for Molecular Sciences, Key Laboratory of Molecular Nanostructure and Nanotechnology, Institute of Chemistry, Chinese Academy of Sciences, Beijing 100190, China

[‡]Beijing National Laboratory for Condensed Matter Physics, CAS Key Laboratory of Soft Matter Physics, Institute of Physics, Chinese Academy of Sciences, Beijing 100190, China

[§]University of Chinese Academy of Sciences, Beijing 100049, China

ABSTRACT: Novel fullerene-based donor-acceptor (DA) dyads, $\text{Sc}_3\text{N@C}_{80}$ -PTZ and C_{60} -PTZ, have been synthesized and investigated, in which the photoinduced electron transfer direction is proved to be switchable by regulating the redox state. In detailed photophysical experiments, reductive electron transfer from PTZ moiety to $\text{Sc}_3\text{N@C}_{80}$ is confirmed with transient absorption (TA) spectroscopy in the neutral $\text{Sc}_3\text{N@C}_{80}$ -PTZ dyad. After oxidizing PTZ moiety to PTZ^+ in a reversible manner, oxidative electron transfer from $\text{Sc}_3\text{N@C}_{80}$ moiety to PTZ^+ radical cation is corroborated experimentally and theoretically, leading to the formation of a metastable charge transfer (CT) state ($\text{Sc}_3\text{N@C}_{80}$)⁺-PTZ, which is not observed in the C_{60} -PTZ⁺ dyad. To the best of our knowledge, this is the first time in-situ tunable molecular photodiode-like behavior is fulfilled utilizing a fullerene dyad. These findings will contribute to the future application of fullerene-based DA conjugates in molecular electronic devices.

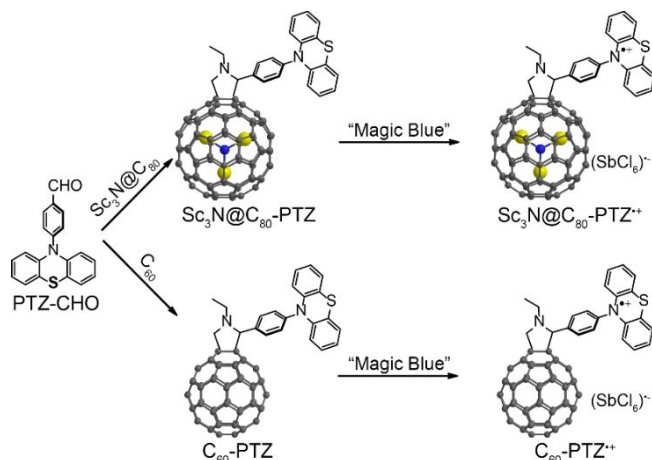
INTRODUCTION

Photoinduced electron transfer (PET), commonly existing in the natural photosynthesis system, is one of the fundamental steps in solar energy conversion.^{1,2} However, further research on fine-tuning of the DA structures and charge transfer behaviors is still demanded.³ The scientific communities have focused interests on designing and synthesizing novel donor-acceptor conjugates, among which fullerene-based DA conjugates have become promising candidates for their unique properties.⁴ In particular, endohedral metallofullerenes (EMFs), with metal atoms or clusters encaged, have variable electronic properties related to the encapsulated species and are widely used as the molecular building units in DA conjugates.⁵⁻⁸ At the beginning of EMFs research in charge transfer chemistry, EMFs play a role as electron-accepting moieties in covalent-linked DA conjugates. In the past few years, EMFs come forth as electron-donating moieties when covalently linked to a strong electron-withdrawing entity, such as perylene-diimides (PDI) and tetracyanoanthraquinodimethane (TCAQ).^{9,10} In particular, previous studies of the $\text{Ce}_2@I_h\text{-C}_{80}$ -ZnP DA conjugate have documented bidirectional charge transfer behavior, namely a reductive electron transfer in nonpolar solution, and an oxidative electron transfer in polar solution, yet the prerequisite of changing solvent polarity might hamper the future applications.¹¹

However, since charge transfer dynamics is partially dominated by the electronic character of exohedral derivative moiety,¹² a new strategy is put forward to fulfill switchable electron transfer dynamic by covalently linking EMFs to a redox-active moiety. Phenothiazine (PTZ), characterized by an anthracene-shaped heterocyclic which bearing a sulfur and nitrogen atom at the central ring, is usually adopted as an electron-donating moiety in electron transfer reactions.¹³⁻¹⁶ However, a remarkably stable one-electron oxidation state of PTZ is accessible in suitable oxidation conditions, in which PTZ^+ shows an electron-withdrawing ability.¹⁷⁻¹⁹ In addition, the physical and chemical properties of PTZ and PTZ^+ are well documented in literature.^{20,21}

In the present work, PTZ was introduced into fullerene-based DA dyads for the first time. *N*-Ethyl-2-(4-(10*H*-phenothiazin-10-yl)phenyl)-[5,6]-*I*_h- $\text{Sc}_3\text{N@C}_{80}$ -fulleropyrrolidine ($\text{Sc}_3\text{N@C}_{80}$ -PTZ), along with C_{60} analog, has been synthesized and investigated with state-of-the-art TA spectroscopy.²² Reductive electron transfer from PTZ moiety to $\text{Sc}_3\text{N@C}_{80}$ was confirmed following laser excitation in the $\text{Sc}_3\text{N@C}_{80}$ -PTZ dyad. However, after the $\text{Sc}_3\text{N@C}_{80}$ -PTZ was reversibly oxidized under suitable oxidation conditions, the oxidative electron transfer process was activated. Photoexcitation of $\text{Sc}_3\text{N@C}_{80}$ -PTZ⁺ gave TA features ascribed to $\text{Sc}_3\text{N@C}_{80}$ radical cation, suggesting ultrafast electron transfer from $\text{Sc}_3\text{N@C}_{80}$ moiety to PTZ^+ , and formation of ($\text{Sc}_3\text{N@C}_{80}$)⁺-PTZ CT state consequently, which was, however, not observed in

C_{60} -PTZ⁺ dyad. In addition, a quantitative investigation according to Marcus theory²³ has shed light on the photophysical process and rationalized the observation of a metastable CT state in $Sc_3N@C_{80}$ -PTZ⁺. To summarize, the overall photoinduced electron transfer direction in the $Sc_3N@C_{80}$ -PTZ dyad has been proven to be in-situ switchable between oxidative/reductive electron transfer.



Scheme 1. Synthesis of neutral C_{60} -PTZ, $Sc_3N@C_{80}$ -PTZ dyads, and C_{60} -PTZ⁺, $Sc_3N@C_{80}$ -PTZ⁺ cation radicals.

RESULTS AND DISCUSSION

Synthesis. The C_{60} and $Sc_3N@I_h-C_{80}$ are synthesized by the Kräschmer – Huffman arc discharge method and isolated using the multi-step high performance liquid chromatography (HPLC).²⁴ The synthesis of $Sc_3N@C_{80}$ -PTZ and C_{60} -PTZ dyads follows the procedure of 1,3-dipolar cycloaddition reaction (Scheme 1), namely the Prato reaction, in which the reactive azomethine ylides generated from the amino acids and the aldehydes condensation react with the double bond on fullerenes.^{25,26} Details of the synthesis, isolation, and characterization are introduced in the Supporting Information. Selective oxidation of PTZ moiety is accomplished using one-electron oxidant, tris(4-bromophenyl)ammoniumyl hexachloroantimonate (“Magic Blue”).^{18, 27} The reduction of PTZ⁺ cation radicals is achieved by adding Zinc powder. For TA measurements, the solvent is removed under reduced pressure, and solutes are redissolved in benzonitrile.

Steady-state absorption. Ground-state absorption spectra of neutral PTZ, C_{60} -PTZ, and $Sc_3N@C_{80}$ -PTZ in dichloromethane are presented in Figure S9. In the neutral state, PTZ shows an intense absorption peak at 320 nm with band edge around 420 nm, while steady-state absorptions of C_{60} -PTZ and $Sc_3N@C_{80}$ -PTZ feature with intense ultraviolet absorption due to the $\pi \rightarrow \pi^*$ transition of fullerene cage π -system and broad absorption band in the visible region.²⁸⁻³⁰

In Figure 1a, upon mixing the “Magic Blue” solution with increasing concentration solution of neutral PTZ, the characteristic absorption band of “Magic Blue” at 730 nm

decreases with a newly-formed absorption peak emerging at 520 nm, which is ascribed to the formation of PTZ⁺ cation radical.^{17,18} At the same time, a similar trend is followed in the case of C_{60} -PTZ and $Sc_3N@C_{80}$ -PTZ, as shown in Figure 1b & 1c, suggesting the formation of C_{60} -PTZ⁺ and $Sc_3N@C_{80}$ -PTZ⁺ cation radicals, respectively.

The reverse reduction of PTZ⁺ cation radical was investigated by inspecting the absorption band at 520 nm. In Figure 1d, the C_{60} -PTZ was firstly oxidized in situ to generate C_{60} -PTZ⁺ with the addition of “Magic blue” in an optical cuvette. Afterward, the typical absorption band at 520 nm fully disappeared with the addition of reductive zinc powder, suggesting complete regeneration of neutral C_{60} -PTZ. Moreover, electrochemical oxidation and reduction of C_{60} -PTZ were also carried out in a homemade spectroelectrochemical cell and the differential absorption spectra were presented in Figure S10, which is alternative access to the regulation of PTZ redox state.¹⁷

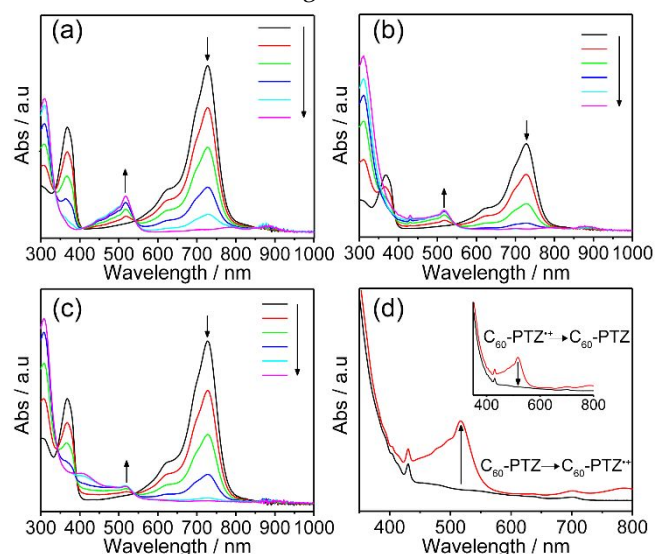


Figure 1. Steady-state absorption spectra of “Magic Blue” solution upon addition increasing amount of (a) PTZ, (b) C_{60} -PTZ, (c) $Sc_3N@C_{80}$ -PTZ in dichloromethane. (d) Steady-state absorption spectra of neutral C_{60} -PTZ and C_{60} -PTZ⁺ in dichloromethane. The inset shows the UV-Vis spectra after the addition of zinc powder. The absorption changes are indicated by the arrows.

Frontier molecular orbital analysis. To gain further understanding of charge transfer characteristics, quantum mechanical (QM) calculations were carried out for elucidating the molecular orbital population of $Sc_3N@C_{80}$ -PTZ, $Sc_3N@C_{80}$ -PTZ⁺, C_{60} -PTZ, and C_{60} -PTZ⁺, respectively (See the Experiment Section for the computational details). The contours of the frontier molecular orbitals (FMOs) are presented in Figure S11 & S12. The highest occupied molecular orbitals of $Sc_3N@C_{80}$ -PTZ and C_{60} -PTZ dyads are predominantly located on the PTZ moiety, while the lowest unoccupied molecular orbitals are substantially contributed by the connected fullerene entities. The nature of the relevant FMOs suggests a great possibility of charge transfer from the PTZ donors to fullerene acceptors. On the other hand, the $Sc_3N@C_{80}$ -

PTZ^{•+} and C₆₀-PTZ^{•+} are significantly different from their neutral analogs. Due to the strong electron-withdrawing ability of the radical cation, the highest occupied beta orbitals are populated on the fullerene, while the lowest unoccupied beta orbitals are localized on the PTZ^{•+} moieties, which suggests that unlike the neutral dyads, the electron is inclined to transfer from the fullerene to the PTZ^{•+} cation radical.

Electrochemistry. Electrochemical properties of PTZ, C₆₀-PTZ, and Sc₃N@C₈₀-PTZ have been investigated by the means of cyclic voltammetry (CV) and differential pulse voltammetry (DPV) in 0.05 M TBAPF₆ 1,2-dichlorobenzene (*o*-DCB) solution. The redox potentials are corrected to ferrocene couple and summarized in Table 1. The cyclic voltammograms and the differential pulse voltammograms are presented in Figure S13 & S14, respectively. PTZ exhibits a reversible one-electron oxidation wave at 0.29 V (vs Fc/Fc⁺), in good agreement with the previous report.¹⁴ In the case of Sc₃N@C₈₀-PTZ, two oxidation waves and three reduction waves are observed. The first reversible oxidation wave at 0.28 V (vs Fc/Fc⁺), which is close to the oxidation potential of PTZ, is attributed to oxidize PTZ moiety. The second oxidation wave at 0.56 V is consistent with the first oxidation potential of intrinsic Sc₃N@C₈₀, corresponding to the oxidation of the Sc₃N@I_h-C₈₀ entity. In the cathodic scan, three reversible reduction waves at -1.20 V, -1.61 V, -2.10 V are displayed for Sc₃N@C₈₀-PTZ dyad, as shown in Figure S15, which are characteristic for [5,6]-I_h-Sc₃N@C₈₀ fulleropyrrolidine adducts.³¹ In general, the electrochemical behaviors of Sc₃N@C₈₀-PTZ show little perturbation comparing to pristine PTZ and Sc₃N@C₈₀, which indicates a limited electronic coupling at the ground state.⁹ A similar redox behavior is also observed in the C₆₀-PTZ dyad.

Table 1. Redox potentials (vs Fc/Fc⁺, in V) of PTZ, C₆₀-PTZ, and Sc₃N@C₈₀-PTZ obtained from CVs and DPVs.

Molecule	oxE ₂	oxE ₁	RedE ₁	RedE ₂	RedE ₃
C ₆₀	-	1.21	-1.12	-1.50	-1.95
C ₆₀ -PTZ	1.20	0.29	-1.18	-	-
Sc ₃ N@C ₈₀	-	0.57	-1.26	-1.62	-2.37
Sc ₃ N@C ₈₀ -PTZ	0.56	0.28	-1.20	-1.61	-2.10
PTZ	-	0.29	-	-	-

According to the redox potentials in Table 1, the driving force ΔG for the charge transfer (CT) and back charge transfer (BCT) processes in Sc₃N@C₈₀-PTZ^{•+} and C₆₀-PTZ^{•+} dyads can be estimated using eq 1 and the results are summarized in Table 2.

Table 2. Calculated ΔG for charge transfer reactions in benzonitrile.

Reactions	$\Delta G^{\circ}(\text{CT})$ / eV	$\Delta G^{\circ}(\text{BCT})$ / eV
Sc ₃ N@C ₈₀ -(PTZ ^{•+}) ^{•+} → [(Sc ₃ N@C ₈₀) ^{•+} -PTZ]	-1.11	-0.28

(Sc ₃ N@C ₈₀) ^{•+} -PTZ ^{•+} → [(Sc ₃ N@C ₈₀) ^{•+} -PTZ]	-1.22	-0.28
C ₆₀ -(PTZ ^{•+}) ^{•+} → [(C ₆₀) ^{•+} -PTZ]	-0.47	-0.92
(C ₆₀) ^{•+} -PTZ ^{•+} → [(C ₆₀) ^{•+} -PTZ]	-0.84	-0.92

Transient absorption spectroscopy. Pump-probe femtosecond TA spectroscopy and nanosecond flash photolysis were utilized to shed light on the ultrafast photoinduced charge transfer dynamics in Sc₃N@C₈₀-PTZ and C₆₀-PTZ dyads. For femtosecond TA analysis, the resulting spectra were imported into Glotaran (a GUI software for the “R” package, “TIMP”) and treated with global analysis to yield evolution associated spectra (EAS) and decay associated spectra (DAS).³²⁻³⁴

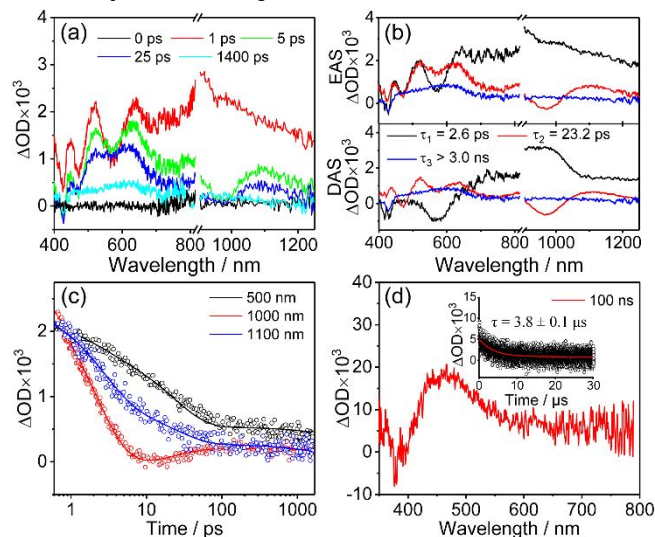


Figure 2. (a) Femtosecond TA spectra of Sc₃N@C₈₀-PTZ in benzonitrile following excitation at 388 nm. (b) EAS and DAS obtained upon global analysis of the transient absorption data. (c) Time-absorption profile at 500 nm (black spectrum), 1000 nm (red spectrum) and 1100 nm (blue spectrum), reflecting the charge separation and recombination dynamics. (d) Nanosecond transient absorption spectra of Sc₃N@C₈₀-PTZ in benzonitrile taken at 100 ns after 355 nm laser pulse excitation and time-absorption profile at 450 nm (inset).

Upon excitation of neutral Sc₃N@C₈₀-PTZ in benzonitrile using a 388 nm laser pulse, TA spectra build up within 1 picosecond, and the corresponding TA spectra with different delay times are presented in Figure 2a. The starting TA spectra feature prominent excited state absorptions (ESA) with maxima at 500 nm, 1000 nm and a minimum at 600 nm, which is in accordance with the differential absorption of singlet excited-state Sc₃N@C₈₀.^{26, 35,36} The first resolved EAS component, therefore, is local excitation (LE) state of fullerene moiety in the Sc₃N@C₈₀-PTZ dyad. The initial singlet excited state features decay fast, as shown in the first DAS spectra, and evolve into the second EAS component associated with the appearance of new ESA maxima at 520 nm, 1100 nm and a minimum at 980 nm. These features bear a great resemblance to the fingerprints of one-electron oxidized PTZ radical cation

and one-electron reduced $\text{Sc}_3\text{N@C}_{80}$ radical anion, respectively.^{26, 29} Consequently, we ascribed the second EAS component to the formation of $(\text{Sc}_3\text{N@C}_{80})^{\cdot-}$ -PTZ⁺ radical ion pair state. As a matter of fact, a singlet excited state lifetime of 2.6 ps has been determined which indicates an effective quenching process as a result of electron transfer from PTZ to singlet excited-state $\text{Sc}_3\text{N@C}_{80}$ moiety, in line with previously reported $\text{Sc}_3\text{N@C}_{80}$ based donor-acceptor dyad.³⁵ Afterward, the radical ion pairs absorption bands decay simultaneously, when a broad ESA peaking at 600 nm appears gradually, and remains unchanged through the entire experiment time range. Nanosecond TA measurements of the dyad in argon-saturated benzonitrile are carried out to verify the long-lived component observed in femtosecond TA measurement, as shown in Figure 2d. Considering the nanosecond TA spectra of $\text{Sc}_3\text{N@C}_{80}$ -PTZ are substantially identical to the pristine $\text{Sc}_3\text{N@C}_{80}$ (Figure S16), the third EAS component is therefore attributed to low-lying triplet excited state of $\text{Sc}_3\text{N@C}_{80}$ via intersystem crossing (ISC), from which a lifetime τ_{ISC} approximately 60 ps is derived (Figure S17). A similar relaxation process is proposed to interpret the photophysical events observed in the C_{60} -PTZ dyad, and the results are presented in Figure S18.^{28, 37}

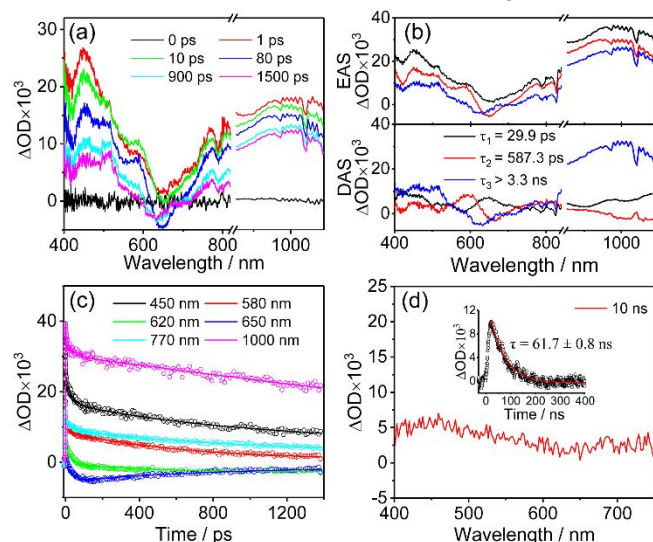


Figure 3. (a) Femtosecond TA spectra of $\text{Sc}_3\text{N@C}_{80}$ -PTZ⁺ cation radical in benzonitrile following excitation at 520 nm. (b) EAS and DAS obtained upon global analysis of the transient absorption data. (c) Time-absorption profile at different wavelengths and fitting curves derived from global analysis. (d) Nanosecond transient absorption of $\text{Sc}_3\text{N@C}_{80}$ -PTZ⁺ cation radical in benzonitrile taken at 10 ns after 520 nm laser pulse excitation and time-absorption profile at 450 nm (inset).

For comparison, femtosecond TA spectra of $\text{Sc}_3\text{N@C}_{80}$ -PTZ⁺ cation radical in benzonitrile were also measured in Figure 3a. However, ESA features attributed to neither singlet excited state $\text{Sc}_3\text{N@C}_{80}$ mentioned above nor PTZ⁺ LE state are observed in the starting TA spectra. In fact, featuring with an intense ESA maximum at 450 nm, a minimum at 650 nm and a broad near-infrared absorption tail, the first EAS component should be ascribed to the

formation of thermodynamics favorable $(\text{Sc}_3\text{N@C}_{80})^{\cdot+}$ -PTZ CT state with a lifetime $\tau_1 = 29.9$ ps, which was investigated in-situ in a spectroelectrochemical experiment.³⁸ Moreover, a weak ground state bleaching (GSB) is discernable at 780 nm which is originated from excited state PTZ⁺ moiety. The initial electron transfer reaction from $\text{Sc}_3\text{N@C}_{80}$ to PTZ⁺ is not discriminated for the reason that it may occur within the instrument response function (IRF) and couldn't be extracted with precision.

The BCT reaction of $(\text{Sc}_3\text{N@C}_{80})^{\cdot+}$ -PTZ state is accompanied by two more components, as shown in Figure 3b. It is worth noting that the third long-lived EAS component bears great resemblance to the first one with the exception of a slight blue shift of the absorption minimum, i.e., from 650 nm to 620 nm, which indicates these components stand for two different relaxation stages of the CT state.³⁹ In fact, charge transfer dynamics of donor-acceptor conjugates with a single-bond linkage usually coexist with concomitant conformational relaxations in high-polarity solvents.³⁹⁻⁴¹

In particular, in the neutral state, the heterocyclic ring of PTZ has a nonplanar geometry, featuring a sp^3 -hybridized character of the nitrogen atom. When in the oxidized state, it adopts a sp^2 hybridization with a more planar geometry,^{15, 18} which is consistent with the QM calculated configurations of the fullerene dyads in Figure S19. Taking the conformational heterogeneity of PTZ into consideration, the second EAS component, therefore, is a transition state from initial “hot” CT state to relaxed CT state with a conformational relaxation time constant $\tau_2 = 587.3$ ps. The relaxed CT state reinstates the ground state with a longer time constant, $\tau_3 = 61.7$ ns, as a result of the conformational twisting.

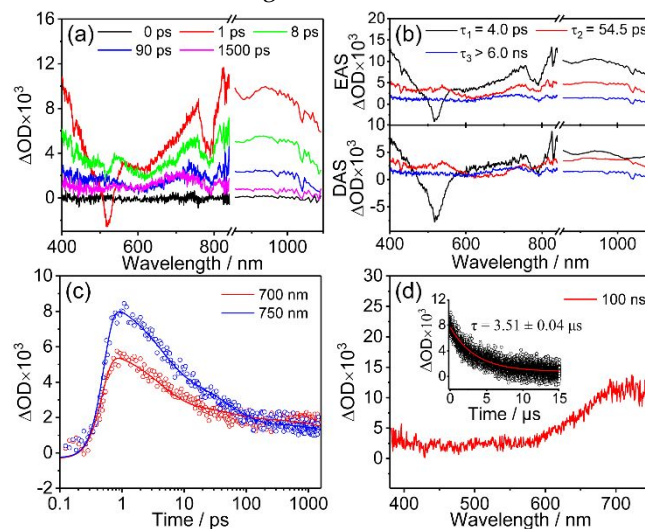


Figure 4. (a) Femtosecond TA spectra of C_{60} -PTZ⁺ cation radical in benzonitrile following excitation at 520 nm. (b) EAS and DAS obtained upon global analysis of the transient absorption data. (c) Time-absorption profile at 700 nm (red spectrum) and 750 nm (blue spectrum), reflecting intersystem crossing dynamics. (d) Nanosecond transient absorption of C_{60} -PTZ⁺ cation radical taken at 100 ns after 520 nm laser pulse excitation and time-absorption profile at 450 nm (inset).

100 ns after 520 nm laser pulse excitation and time-absorption profile at 700 nm (inset).

Table 3. The charge transfer reaction parameters for C_{60} -PTZ⁺ and $Sc_3N@C_{80}$ -PTZ⁺ cation radical derived from theoretical calculations and experiments.

Reactions	λ_i (eV)	λ_s (eV)	λ (eV)	G° (eV)	V (eV)	k_{CT} (s ⁻¹)	τ_{cal} (ps)	τ_{exp} (ps)
$Sc_3N@C_{80}-(PTZ^+)^* \rightarrow [(Sc_3N@C_{80})^+-PTZ]$	0.4509	0.8600	1.3109	-1.1100	-0.0443	$2.13E+13$	0.0470	-
$(Sc_3N@C_{80})^--PTZ^+ \rightarrow [(Sc_3N@C_{80})^+-PTZ]$	0.4509	0.8600	1.3109	-1.2200	0.0457	$2.87E+13$	0.0348	-
$C_{60}-(PTZ^+)^* \rightarrow [(C_{60})^+-PTZ]$	0.4526	0.9000	1.3526	-0.4700	-0.0384	$8.11E+10$	12.3358	-
$(C_{60})^--PTZ^+ \rightarrow [(C_{60})^+-PTZ]$	0.4526	0.9000	1.3526	-0.8400	-0.2030	$9.06E+13$	0.0110	-
$[(Sc_3N@C_{80})^+-PTZ] \rightarrow Sc_3N@C_{80}-PTZ^+$	0.3164	1.1764	0.8600	-0.2800	0.0457	$4.36E+10$	22.9252	29.9
$[(C_{60})^+-PTZ] \rightarrow C_{60}-PTZ^+$	0.4338	1.3338	0.9000	-0.9200	-0.2030	$1.73E+14$	0.0058	-

In addition, C_{60} -PTZ⁺ cation radical in benzonitrile is subjected to a 520 nm laser excitation, and the consequent femtosecond TA spectra are presented in Figure 4a. The initial TA spectra are dominated by a strong GSB band at 520 nm, a weak GSB negative peak at 780 nm, and a broad near-infrared ESA band around 900 nm. The former is ascribed to the formation of doublet excited state of PTZ⁺, while the latter is assigned to singlet excited state transition ($S_1 \rightarrow S_n$) features of C_{60} fulleropyrrolidine.^{18, 28} The first resolved EAS component for C_{60} -PTZ⁺, therefore, is the combination of $^2PTZ^+$ and $^1(C_{60})^*$, with a time constant $\tau_1 = 4.0$ ps. The starting GSB band at 520 nm and 780 nm recovery rapidly with the appearance of an ESA band around 500 nm within 10 ps, without any discernible peak shift. As a result, we ascribed the second EAS component to relaxed $^2PTZ^+$ and $^1(C_{60})^*$, featuring a much weak GSB at 520 nm and two ESA bands at 500 nm, 900 nm respectively.^{18, 28} The remaining $^1(C_{60})^*$ decays through ISC to produce the third EAS component of $^3(C_{60})^*$ with characteristic absorption at 700 nm. The long-lived component recovery to the ground state with a time constant $\tau = 3.51$ μ s, as shown in Figure 4d, close to a typical C_{60} triplet lifetime.⁴² It should be noted that charge transfer from either C_{60} singlet/triplet excited state or PTZ doublet excited state to $(C_{60})^+-PTZ$ is thermodynamically feasible, as shown in Table 2, but no TA spectra ascribed to $(C_{60})^+$ cation radical ($\lambda_{max} = 980$ nm) is resolved out in femtosecond TA measurements.⁴³

Kinetics for the Charge Transfer Reactions. To further comprehend the experimental results obtained in the femtosecond TA measurements, we quantitatively discuss the CT and BCT reactions in C_{60} -PTZ⁺ and $Sc_3N@C_{80}$ -PTZ⁺ cation radical with the Marcus equation.²³ The driving force G° was obtained from Table 2, and other related values and the kinetic parameters are calculated with the theoretical method. Eventually, the rate constant k_{CT} and k_{BCT} for both C_{60} and EMF dyads are calculated and listed in Table 3.

For both C_{60} -PTZ⁺ and $Sc_3N@C_{80}$ -PTZ⁺ cation radical, the CT & BCT process is located in the normal region of the Marcus parabola.^{44,45} Evidently, the CT process in

$Sc_3N@C_{80}$ -PTZ⁺ is more efficient than C_{60} -PTZ⁺ upon selective excitation of PTZ⁺ moiety using 520 nm laser irradiation, ultrafast electron transfer from $Sc_3N@C_{80}$ moiety to PTZ⁺ is theoretically corroborated. For the BCT process, the significant difference between driving force and reorganization energy, plus the weak electronic coupling are two key factors that together contribute to a much slower BCT rate, viz. a more stable CT state in the EMF derivative. The calculated lifetime of the $(Sc_3N@C_{80})^+-PTZ$ CT state in the dyad is 22.9 ps, which is in good agreement of the 29.9 ps lifetime obtained from the femtosecond TA experiment. The C_{60} system, on the other hand, has a very fast BCT process which could be hardly observed from the experiments.

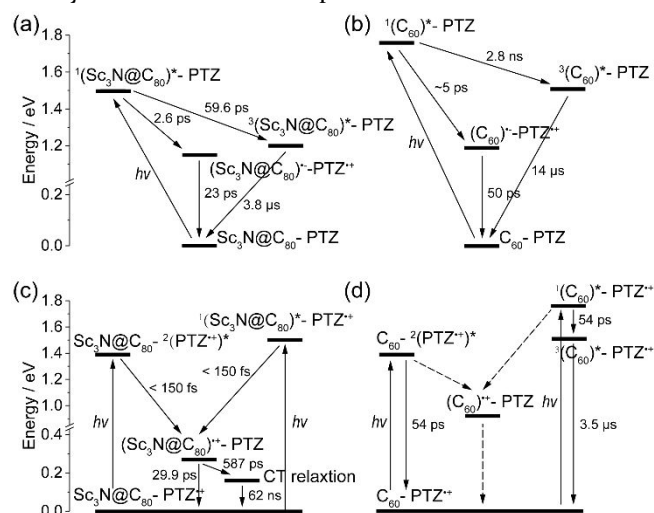


Figure 5. Jablonski diagrams and photophysical dynamics of (a) $Sc_3N@C_{80}$ -PTZ, (b) C_{60} -PTZ, (c) $Sc_3N@C_{80}$ -PTZ⁺, (d) C_{60} -PTZ⁺ after laser pump excitation.

Figure 5 highlights the energy level diagrams and photophysical kinetics for $Sc_3N@C_{80}$ -PTZ, $Sc_3N@C_{80}$ -PTZ⁺ cation radical, C_{60} -PTZ and C_{60} -PTZ⁺ cation radical, respectively. As a matter of fact, in addition to ISC, a CT-mediated relaxation pathway is suggested to be responsible for excited-state dynamics of neutral C_{60} -PTZ and $Sc_3N@C_{80}$ -PTZ dyads, as shown in Figure 5a & 5b. Following laser excitation, the singlet-excited-state

features of $\text{Sc}_3\text{N@C}_{80}$ at 1.50 eV is quenched rapidly with the appearance of $(\text{Sc}_3\text{N@C}_{80})^{\cdot-}$ -PTZ $^{\cdot+}$ CT state at 1.15 eV, as a result of ultrafast electron transfer ($k_{\text{CT}} = 3.8 \times 10^{11} \text{ s}^{-1}$) from PTZ to $^1(\text{Sc}_3\text{N@C}_{80})^*$.³⁵ Subsequent charge recombination ($k_{\text{CR}} = 4.3 \times 10^{10} \text{ s}^{-1}$) directly gives the population of ground state, leaving the triplet excited state of $\text{Sc}_3\text{N@C}_{80}$ (1.20 eV) as final observed component. However, a distinct charge transfer behavior is activated after oxidizing $\text{Sc}_3\text{N@C}_{80}$ -PTZ to $\text{Sc}_3\text{N@C}_{80}$ -PTZ $^{\cdot+}$ cation radical. A low-lying CT state at 0.28 eV is efficiently populated, suggesting ultrafast electron transfer from $\text{Sc}_3\text{N@C}_{80}$ to PTZ $^{\cdot+}$ ($k_{\text{CT}} > 3.3 \times 10^{12} \text{ s}^{-1}$). At the same time, back charge transfer to the ground state almost slows down by two orders of magnitude ($k_{\text{CR}} = 7.8 \times 10^{10} \text{ s}^{-1}$), accompanied by a conformational relaxation of PTZ moiety, leading to the stabilization $(\text{Sc}_3\text{N@C}_{80})^{\cdot+}$ -PTZ CT state. In contrast, the $(\text{C}_{60})^{\cdot+}$ -PTZ transient species should never be accumulated for the reason that its rate of formation is slower than relaxation to the ground state (indicating by dotted line arrows) according to theoretical calculation.

Combining TA spectra and energetic results together, it is possible to conclude that the charge transfer behaviors of fullerene linked to a redox-active PTZ moiety could be in-situ manipulated by simply regulating the redox condition.

CONCLUSION

To summarize, we have successfully synthesized two novel fullerene dyads featuring redox-active PTZ moieties as counterparts. The neutral PTZ moiety is capable of reversibly converting to stable PTZ $^{\cdot+}$ cation radical, which bears significantly different electronic structure compared to its neutral state. State-of-the-art TA measurements have been employed to unveil their photoinduced excited-state dynamics. By regulating the redox state of PTZ, we have realized full control of the photoinduced electron transfer direction in the dyads. This is, to the best of our best knowledge, the first time that a fullerene-based dyad shows in-situ tunable molecular photodiode-like behaviors.¹¹ Our findings suggest a new implement of endohedral metallofullerene in novel molecular electronics devices.

EXPERIMENTAL SECTION

General Methods. All chemical reagents were purchased from a commercial supplier and used as received unless otherwise noted. $\text{Sc}_3\text{N@I}_h\text{-C}_{80}$ was synthesized with the arc-discharge method and isolated with HPLC. Preparative HPLC was performed on a $10 \times 250 \text{ mm}$ Buckprep column with toluene as eluent. All reactions were carried out in Argon atmosphere using standard Schlenk techniques. ^1H NMR spectra were measured on a Bruker Avance-400 spectrometer with chemical shifts reported in ppm relative to the solvent peak. Mass spectra were recorded on Shimadzu MALDI-TOF-MS Spectrometer with 1,9,10-trihydronaphthalene as the matrix. UV-Vis absorption spectra were recorded on a Lambda 950 spectrophotometer (PerkinElmer, U.S.A.).

Electrochemistry. The cyclic voltammetry measurements were performed on a Shanghai Chenhua CHI660C electrochemical analyzer. Experiments were carried out in *o*-DCB at room temperature, using 0.05 M TBAPF $_6$ as supporting electrolyte and a scan rate of 50 mV/s. A silver wire was used as the reference electrode, a platinum wire was used as the counter electrode, and a glassy carbon electrode was used as the working electrode after polished with alumina suspension, rinsed with deionized water and dichloromethane. The ferrocene/ferrocenium redox potential was used as the internal standard reference.

Transient Absorption Measurements. Femtosecond TA measurements were carried out on a homemade spectroscopy setup. The laser source was a commercial femtosecond amplifier laser system (35 fs, 1 kHz, 800 nm, Spitfire Ace, Spectra Physics). The output pulse was split into two beams. The first beam was used to pump a commercial wavelength conversion system (TOPAS prime and wavelength mixing unit from Spectra Physics) which will output tunable femtosecond laser pulses from 350 nm to 2600 nm. The pulses centered at 517 nm and 387 nm were selected as the excitation pulse. The second beam with weaker energy was focused on a CaF $_2$ plate (4 mm thickness) or an yttrium aluminum garnet plate to generate a white light continuum for the visible or near-infrared probe, respectively. The time delay between the pump beam and the probe pulses was controlled by a motorized delay stage. In the case of the visible transient absorption experiment, a laser frequency synchronized fiber optical spectrometer (AvaSpec-ULS2048CL-EVO, Avantes) was used to collect the probe light. For the near-infrared transient signal acquisition, a homemade 46 channel lock-in amplifier coupled spectrometer was utilized. During the experiment, the pump intensity was set to be 350 $\mu\text{J}/\text{cm}^2$ and 1 mJ/cm^2 for the 388 nm and 520 nm laser pulses.

Nanosecond-to-microsecond transient absorption experiments were performed using a commercial nanosecond laser flash photolysis spectrometer (LP980-KS, Edinburgh Instruments Ltd., Livingston, UK) at ambient temperature. The pump laser pulse was obtained either from the third harmonics generation Nd:YAG laser (Quanta-Ray LAB190, Spectra-Physics) at 355 nm or from Optical Parametric Oscillator (PrimoScan ULD400, Spectra-Physics) at 520 nm, with the fwhm of no more than 10 ns. The probe light was provided by a 150 W pulsed xenon arc lamp. The sample solution in $1 \times 1 \text{ cm}$ optical glass cuvette was excited by the pump laser, afterward, the probe light from the xenon lamp passed through the sample in a right-angle configuration. The transmission probe light was measured either by a single PMT detector (Hamamatsu R928), using a Tektronix Model MDO3052 (100 MHz, 1.25 GSs^{-1}) digital oscilloscope, at a specified wavelength for kinetic analysis or by an ICCD camera (DH320T, Andor) for spectral analysis.

All samples were freshly prepared and deaerated for 20 min with argon prior to transient absorption investigation.

Computational Methodology.

Driving force

The Gibbs free energy change for electron transfer reaction in benzonitrile, namely driving force is directly calculated using the following equation:

$$\Delta G(\text{BCT}) = -(E_{\text{ox}}(\text{fullerene}) - E_{\text{ox}}(\text{PTZ}))$$

$$\Delta G(\text{CT}) = -\Delta G(\text{BCT}) - E_{0,0} \quad (1)$$

where the $E_{\text{ox}}(\text{fullerene})$ and $E_{\text{ox}}(\text{PTZ})$ are the oxidation potentials of studied fullerenes and the PTZ, respectively. $E_{0,0}$ refers to the molecular zero-zero transition energy of excited chromophore. We left out the Coulomb interactions and reorganization energy for the reason that the overall charge number remains constant during charge transfer reactions and the tests are carried out in high polarity solvent.

Marcus Equation

The rate of the charge transfer reactions can be calculated with the Marcus equation as following:

$$k_{\text{CT}} = \frac{2\pi}{\hbar} V^2 \frac{1}{\sqrt{4\pi\lambda kT}} \exp\left[-\frac{(\Delta G^0 + \lambda)^2}{4\lambda kT}\right] \quad (2)$$

In which ΔG^0 , λ , and V are the driving force, reorganization energy, and the electron coupling items. The ΔG^0 values of both CT and BCT processes were obtained from the electrochemistry measurement results. Meanwhile, the λ is composed of the inner reorganization energy (λ_i) and the solvent reorganization energy (λ_s).

$$\lambda = \lambda_i + \lambda_s \quad (3)$$

The λ_i is caused by geometric relaxation of the charge transfer state, which can be obtained from the DFT calculated result of the energy difference between the adiabatic ($E_{\text{adia.}}$) and the vertical ($E_{\text{vert.}}$) transition state.

$$\lambda_i = E_{\text{vert.}} - E_{\text{adia.}} \quad (4)$$

Meanwhile, the λ_s can be calculated via the Dielectric Continuum model:

$$\lambda_s = \frac{e^2}{4\pi\epsilon_0} \left[\left(\frac{1}{R_+} + \frac{1}{R_-} - \frac{1}{R_D - a} \right) \left(\frac{1}{n^2} + \frac{1}{\epsilon_s} \right) \right] \quad (5)$$

In which the R_+ , R_- , R_{DA} , n , and ϵ_s are the van der-Waals radius of the donor and acceptor, the center-center distance between the donor and the acceptor, the refractive index and the static dielectric constant of the solvent, respectively. The conformational details are obtained from the QM calculations.

GMH Method

The electron coupling (V) can be calculated with the Generalized Mulliken-Hush method⁴⁶

$$V_{12} = \frac{\mu_{12}\Delta E_{12}}{\sqrt{\Delta\mu_{12}^2 + 4\mu_{12}^2}} \quad (6)$$

Where μ_{12} , $\Delta\mu_{12}$, and ΔE_{12} are the diabatic dipole transition moment, the dipole moment difference of the diabatic states and the vertical excitation energy, respectively. The code implemented in the ECoupling Server⁴⁷ can be used to calculate the V value with GMH method by uploading the calculation result of the

optimized structure of the fullerene derivatives. Reasonable results have been obtained in the previously reported articles.

Quantum Chemical Calculation Details

The density functional (DFT) method implemented in Gaussian 09 package⁴⁸ was adopted for elucidating the CT mechanism of the fullerene-PTZ/PTZ⁺ systems. The geometry of the C₆₀-PTZ, C₆₀-PTZ⁺, Sc₃N@C₈₀-PTZ and Sc₃N@C₈₀-PTZ⁺ systems were optimized with the B₃LYP functional. The 6-31G(d) basis set is applied to the C, H, N, S elements and the SDD basis set is used to describe the Sc element. Frequency analysis was further conducted and no imaginary frequencies were found in any of the systems. The vertical and adiabatic (geometric relaxed) CT state energy is calculated with the time-dependent density functional (TDDFT) method with the Mo6-2X functional with the same basis sets employed as in the geometry optimizations.

ASSOCIATED CONTENT

Supporting Information.

The Support Information is available free of charge via the Internet at <http://pubs.acs.org>.

Experimental details and characterization data.

AUTHOR INFORMATION

Corresponding Author

* E-mail: zkywubo@iccas.ac.cn

* E-mail: yxweng@iphy.ac.cn

* E-mail: crwang@iccas.ac.cn

Author Contributions

†These authors contributed equally.

Notes

The authors declare no competing financial interest.

ACKNOWLEDGMENT

This work was supported by the National Natural Science Foundation of China (51772300, 51832008), Beijing Natural Science Foundation (2182094). B. Wu particularly thanks the Youth Innovation Promotion Association of CAS (2018039).

REFERENCES

- Gust, D.; Moore, T. A.; Moore, A. L. Solar fuels via artificial photosynthesis. *Acc. Chem. Res.* **2009**, *42*, 1890-1898.
- Wasielewski, M. R. Photoinduced electron transfer in supramolecular systems for artificial photosynthesis. *Chem. Rev.* **1992**, *92*, 435-461.
- El-Khouly, M. E.; El-Mohsnawy, E.; Fukuzumi, S. Solar energy conversion: From natural to artificial photosynthesis. *J. Photochem. Photobiol., C* **2017**, *31*, 36-83.
- Imahori, H.; Sakata, Y. Donor-Linked Fullerenes: Photoinduced electron transfer and its potential application. *Adv. Mater.* **1997**, *9*, 537-546.
- Zieleniewska, A.; Lodermeier, F.; Roth, A.; Guldi, D. M. Fullerenes - how 25 years of charge transfer chemistry have shaped our understanding of (interfacial) interactions. *Chem. Soc. Rev.* **2018**, *47*, 702-714.

6. Popov, A. A.; Yang, S.; Dunsch, L. Endohedral fullerenes. *Chem. Rev.* **2013**, *113*, 5989-6113.
7. Yang, S.; Wei, T.; Jin, F. When metal clusters meet carbon cages: endohedral clusterfullerenes. *Chem. Soc. Rev.* **2017**, *46*, 5005-5058.
8. Lu, X.; Feng, L.; Akasaka, T.; Nagase, S. Current status and future developments of endohedral metallofullerenes. *Chem. Soc. Rev.* **2012**, *41*, 7723-7760.
9. Rudolf, M.; Feng, L.; Slanina, Z.; Akasaka, T.; Nagase, S.; Guldi, D. M. A metallofullerene electron donor that powers an efficient spin flip in a linear electron donor-acceptor conjugate. *J. Am. Chem. Soc.* **2013**, *135*, 11165-11174.
10. Takano, Y.; Obuchi, S.; Mizorogi, N.; Garcia, R.; Herranz, M. A.; Rudolf, M.; Guldi, D. M.; Martin, N.; Nagase, S.; Akasaka, T. An endohedral metallofullerene as a pure electron donor: intramolecular electron transfer in donor-acceptor conjugates of La₂@C₈₀ and 11,11,12,12-tetracyano-9,10-anthra-p-quinodimethane (TCAQ). *J. Am. Chem. Soc.* **2012**, *134*, 19401-19408.
11. Yasutomi, S.; Morita, T.; Imanishi, Y.; Kimura, S. A molecular photodiode system that can switch photocurrent direction. *Science* **2004**, *304*, 1944-1947.
12. Prato, M.; Maggini, M. Fulleropyrrolidines: A Family of Full-Fledged Fullerene Derivatives. *Acc. Chem. Res.* **1998**, *31*, 519-526.
13. Daub, J.; Engl, R.; Kurzawa, J.; Miller, S. E.; Schneider, S.; Stockmann, A.; Wasielewski, M. R. Competition between Conformational Relaxation and Intramolecular Electron Transfer within Phenothiazine-Pyrene Dyads. *J. Phys. Chem. A* **2001**, *105*, 5655-5665.
14. Lee, S. H.; Chan, C. T.; Wong, K. M.; Lam, W. H.; Kwok, W. M.; Yam, V. W. Design and synthesis of bipyridine platinum(II) bisalkynyl fullerene donor-chromophore-acceptor triads with ultrafast charge separation. *J. Am. Chem. Soc.* **2014**, *136*, 10041-10052.
15. Knorr, A.; Daub, J. Luminescence Stimulated by Electron Transfer: Fluorescent Donor/Acceptor-Substituted Stilbenes Containing Pyrenoid and Heteroaromatic Subunits. *Angew. Chem. Int. Ed.* **1996**, *34*, 2664-2666.
16. Knorr, A.; Daub, J. Structural Reorganization of Anthracene-Bridged Stilbenoids by Oxidation and Reduction. *Angew. Chem. Int. Ed.* **1997**, *36*, 2817-2819.
17. Satoh, Y.; Catti, L.; Akita, M.; Yoshizawa, M. A Redox-Active Heterocyclic Capsule: Radical Generation, Oxygenation, and Guest Uptake/Release. *J. Am. Chem. Soc.* **2019**, *141*, 12268-12273.
18. Christensen, J. A.; Phelan, B. T.; Chaudhuri, S.; Acharya, A.; Batista, V. S.; Wasielewski, M. R. Phenothiazine Radical Cation Excited States as Super-oxidants for Energy-Demanding Reactions. *J. Am. Chem. Soc.* **2018**, *140*, 5290-5299.
19. Sun, D.; Rosokha, S. V.; Kochi, J. K. Donor-acceptor (electronic) coupling in the precursor complex to organic electron transfer: intermolecular and intramolecular self-exchange between phenothiazine redox centers. *J. Am. Chem. Soc.* **2004**, *126*, 1388-1401.
20. Liu, J.; Zhao, X.; Al-Galiby, Q.; Huang, X.; Zheng, J.; Li, R.; Huang, C.; Yang, Y.; Shi, J.; Manrique, D. Z.; Lambert, C. J.; Bryce, M. R.; Hong, W. Radical-Enhanced Charge Transport in Single-Molecule Phenothiazine Electrical Junctions. *Angew. Chem. Int. Ed.* **2017**, *56*, 13061-13065.
21. Pelizzetti, E.; Mentasti, E. Cation radicals of phenothiazines. Electron transfer with aquoiron(II) and -(III) and hexacyanoferrate(II) and -(III). *Inorg. Chem.* **1979**, *18*, 583-588.
22. Chi, Z.; Chen, H.; Chen, Z.; Zhao, Q.; Chen, H.; Weng, Y. X. Ultrafast Energy Dissipation via Coupling with Internal and External Phonons in Two-Dimensional MoS₂. *ACS Nano* **2018**, *12*, 8961-8969.
23. Marcus, R. A.; Sutin, N. Electron transfers in chemistry and biology. *Biochim. Biophys. Acta, Rev. Bioenerg.* **1985**, *811*, 265-322.
24. Krätschmer, W.; Lamb, L. D.; Fostiropoulos, K.; Huffman, D. R. Solid C₆₀: a new form of carbon. *Nature* **1990**, *347*, 354-358.
25. Maggini, M.; Scorrano, G.; Prato, M. Addition of azomethine ylides to C₆₀: synthesis, characterization, and functionalization of fullerene pyrrolidines. *J. Am. Chem. Soc.* **1993**, *115*, 9798-9799.
26. Pinzon, J. R.; Plonska-Brzezinska, M. E.; Cardona, C. M.; Athans, A. J.; Gayathri, S. S.; Guldi, D. M.; Herranz, M. A.; Martin, N.; Torres, T.; Echegoyen, L. Sc₃N@C₈₀-ferrocene electron-donor/acceptor conjugates as promising materials for photovoltaic applications. *Angew. Chem. Int. Ed.* **2008**, *47*, 4173-4176.
27. Walter, R. I. Substituent Effects on the Properties of Stable Aromatic Free Radicals. The Criterion for Non-Hammett Behavior. *J. Am. Chem. Soc.* **1966**, *88*, 1923-1930.
28. Guldi, D. M.; Prato, M. Excited-state properties of C₆₀ fullerene derivatives. *Acc. Chem. Res.* **2000**, *33*, 695-703.
29. Liu, B.; Fang, H.; Li, X.; Cai, W.; Bao, L.; Rudolf, M.; Plass, F.; Fan, L.; Lu, X.; Guldi, D. M. Synthesis and photophysical properties of a Sc₃N@C₈₀-corrole electron donor-acceptor conjugate. *Chem. Eur. J.* **2015**, *21*, 746-752.
30. Krause, M.; Dunsch, L. Isolation and characterisation of two Sc₃N@C₈₀ isomers. *ChemPhysChem* **2004**, *5*, 1445-1449.
31. Cardona, C. M.; Elliott, B.; Echegoyen, L. Unexpected chemical and electrochemical properties of M₃N@C₈₀ (M = Sc, Y, Er). *J. Am. Chem. Soc.* **2006**, *128*, 6480-6485.
32. Hippus, C.; van Stokkum, I. H. M.; Zangrando, E.; Williams, R. M.; Würthner, F. Excited State Interactions in Calix[4]arene-Perylene Bisimide Dye Conjugates: Global and Target Analysis of Supramolecular Building Blocks. *J. Phys. Chem. C* **2007**, *111*, 13988-13996.
33. Mullen, K. M.; Stokkum, I. H. M. TIMP: An R Package for Modeling Multi-Way Spectroscopic Measurements. *J. Stat. Softw.* **2007**, *18*, 1-46.
34. van Stokkum, I. H.; Larsen, D. S.; van Grondelle, R. Global and target analysis of time-resolved spectra. *Biochim. Biophys. Acta.* **2004**, *1657*, 82-104.
35. Pinzon, J. R.; Gasca, D. C.; Sankaranarayanan, S. G.; Bottari, G.; Torres, T.; Guldi, D. M.; Echegoyen, L. Photoinduced charge transfer and electrochemical properties of triphenylamine I_h-Sc₃N@C₈₀ donor-acceptor conjugates. *J. Am. Chem. Soc.* **2009**, *131*, 7727-7734.
36. Wolfsum, S.; Pinzon, J. R.; Molina-Ontoria, A.; Gouloumis, A.; Martin, N.; Echegoyen, L.; Guldi, D. M. Utilization of Sc₃N@C₈₀ in long-range charge transfer reactions. *Chem. Commun.* **2011**, *47*, 2270-2272.
37. de Miguel, G.; Wielopolski, M.; Schuster, D. I.; Fazio, M. A.; Lee, O. P.; Haley, C. K.; Ortiz, A. L.; Echegoyen, L.; Clark, T.; Guldi, D. M. Triazole bridges as versatile linkers in electron donor-acceptor conjugates. *J. Am. Chem. Soc.* **2011**, *133*, 13036-13054.
38. Popov, A. A.; Shustova, N. B.; Svitova, A. L.; Mackey, M. A.; Coumbe, C. E.; Phillips, J. P.; Stevenson, S.; Strauss, S. H.; Boltalina, O. V.; Dunsch, L. Redox-tuning endohedral fullerene spin states: from the dication to the trianion radical of Sc₃N@C₈₀(CF₃)₂ in five reversible single-electron steps. *Chem. Eur. J.* **2010**, *16*, 4721-4724.
39. Kuang, Z.; He, G.; Song, H.; Wang, X.; Hu, Z.; Sun, H.; Wan, Y.; Guo, Q.; Xia, A. Conformational Relaxation and Thermally Activated Delayed Fluorescence in Anthraquinone-Based Intramolecular Charge-Transfer Compound. *J. Phys. Chem. C* **2018**, *122*, 3727-3737.

40. Niu, X.; Gautam, P.; Kuang, Z.; Yu, C. P.; Guo, Y.; Song, H.; Guo, Q.; Chan, J. M. W.; Xia, A. Intramolecular charge transfer and solvation dynamics of push-pull dyes with different pi-conjugated linkers. *Phys. Chem. Chem. Phys.* **2019**, *21*, 17323-17331.
41. Choi, J.; Ahn, D.-S.; Oang, K. Y.; Cho, D. W.; Ihee, H. Charge Transfer-Induced Torsional Dynamics in the Excited State of 2,6-Bis(diphenylamino)anthraquinone. *J. Phys. Chem. C* **2017**, *121*, 24317-24323.
42. Kajii, Y.; Nakagawa, T.; Suzuki, S.; Achiba, Y.; Obi, K.; Shibuya, K. Transient absorption, lifetime and relaxation of C₆₀ in the triplet state. *Chem. Phys. Lett.* **1991**, *181*, 100-104.
43. Biczók, L.; Linschitz, H. Oxidation of Triplet C₆₀ by Hydrogen-Bonded Chloranil: Efficient Formation, Spectrum and Charge-Shift Reactions of C₆₀^{•+} Cation Radical. *J. Phys. Chem. A* **2001**, *105*, 11051-11056.
44. Fukuzumi, S.; Ohkubo, K.; Suenobu, T. Long-lived charge separation and applications in artificial photosynthesis. *Acc. Chem. Res.* **2014**, *47*, 1455-1464.
45. Imahori, H.; Tamaki, K.; Guldi, D. M.; Luo, C.; Fujitsuka, M.; Ito, O.; Sakata, Y.; Fukuzumi, S. Modulating charge separation and charge recombination dynamics in porphyrin-fullerene linked dyads and triads: Marcus-normal versus inverted region. *J. Am. Chem. Soc.* **2001**, *123*, 2607-26017.
46. Cave, R. J.; Newton, M. D. Generalization of the Mulliken-Hush treatment for the calculation of electron transfer matrix elements. *Chem. Phys. Lett.* **1996**, *249*, 15-19.
47. Cabeza de Vaca, I.; Acebes, S.; Guallar, V. Ecoupling Server: A Tool to Compute and Analyze Electronic Couplings. *J. Comput. Chem.* **2016**, *37*, 1740-1745.
48. Frisch, M. J.; Trucks, G. W.; Schlegel, H. B.; Scuseria, G. E.; Robb, M. A.; Cheeseman, J. R.; Scalmani, G.; Barone, V.; Mennucci, B.; Petersson, G. A.; Nakatsuji, H.; Caricato, M. Gaussian 09, d.01; Gaussian, Inc.: Wallingford CT, **2013**.

